Supplementary material

Text S1. Environmental characteristics of seasonal snow in northeastern and northwestern China

Snow physicochemical properties differed between northeastern (NE) and northwestern (NW) China (Table S1). The mean TOC concentration was markedly higher in NE snow than in NW snow (18.055 ± 7.079 vs. 1.744 ± 1.442 mg L^{-1}, $p < 0.001$), as was the NH_4^+ concentration (2.032 ± 1.308 mg L^{-1} vs. 1.216 ± 1.370 mg L^{-1}, $p < 0.05$). The mean TOC concentration in NE snow exceeded values reported for surface snow on the Tibetan Plateau (1.19 ± 1.78 mg L^{-1}) and at the South Pole (400 ± 130 μg^{-1}) (Grannas et al., 2004; Liu et al., 2022). The higher TOC and NH_4^+ concentration in NE snow was consistent with stronger inputs from regional agricultural activities, biomass burning, and industrial emissions (Murphy et al., 2008; Fourtziou et al., 2017; Mu et al., 2023). K^+ and SO_4^{2-} also differed between regions ($p < 0.001$ and $p < 0.05$, respectively). Both ions were far more variable in NW snow (K^+: 1.256 ± 5.075 mg L^{-1}; SO_4^{2-}: 44.225 ± 198.261 mg L^{-1}) than in NE snow (K^+: 0.694 ± 0.366 mg L^{-1}; SO_4^{2-}: 8.180 ± 5.608 mg L^{-1}), largely because of the high values in XJ.Q402. The mean NO_3^- concentration was higher in NW snow (3.658 ± 2.849 mg L^{-1} vs. 2.416 ± 1.455 mg L^{-1}), but the regional difference was not significant ($p = 0.20$). Anthropogenic emissions may contribute to nitrate deposition in NE China (Luo et al., 2019), whereas atmospheric photochemistry and in-snow microbial transformations may also contribute to nitrate in NW snow (Amoroso et al., 2010; Fourtziou et al., 2017; Zatko et al., 2016).

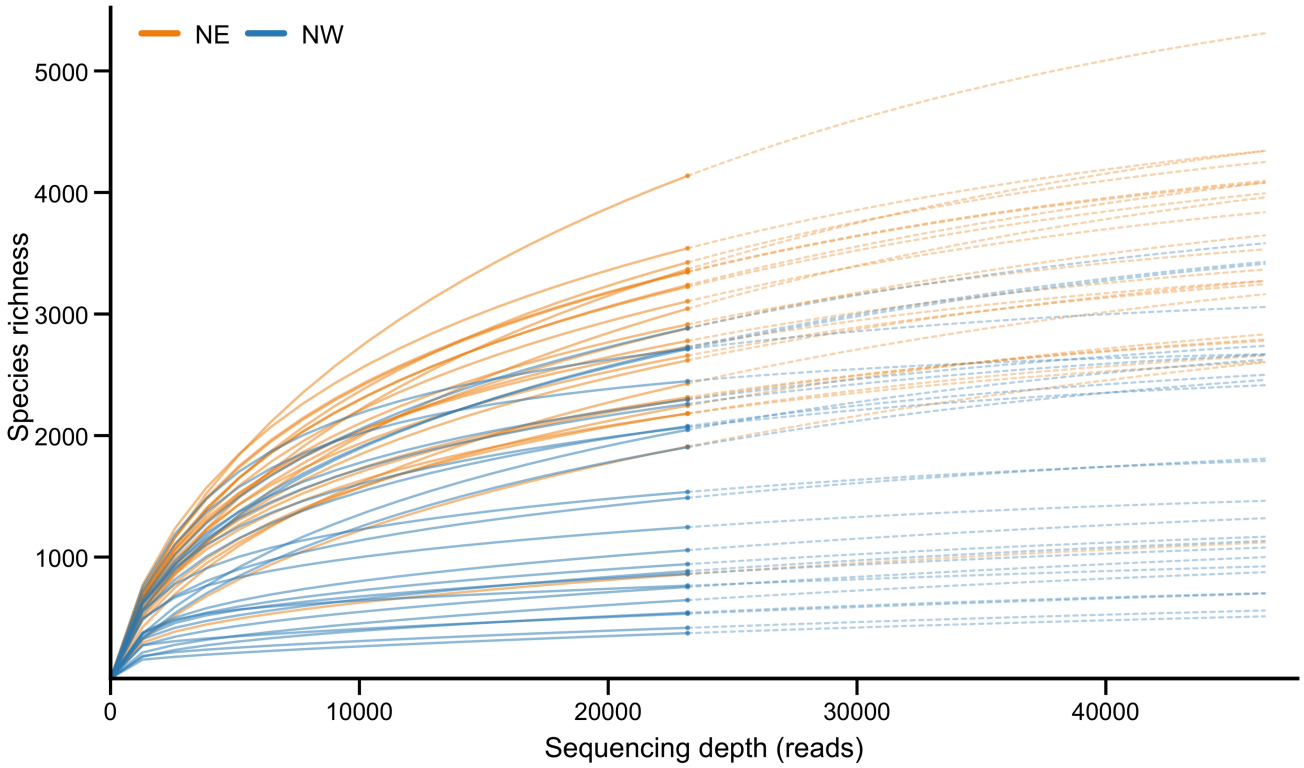


Fig. S1. Sample-based rarefaction (solid lines) and extrapolation (dotted lines) of bacterial species richness ($q = 0$) in NE and NW snow.

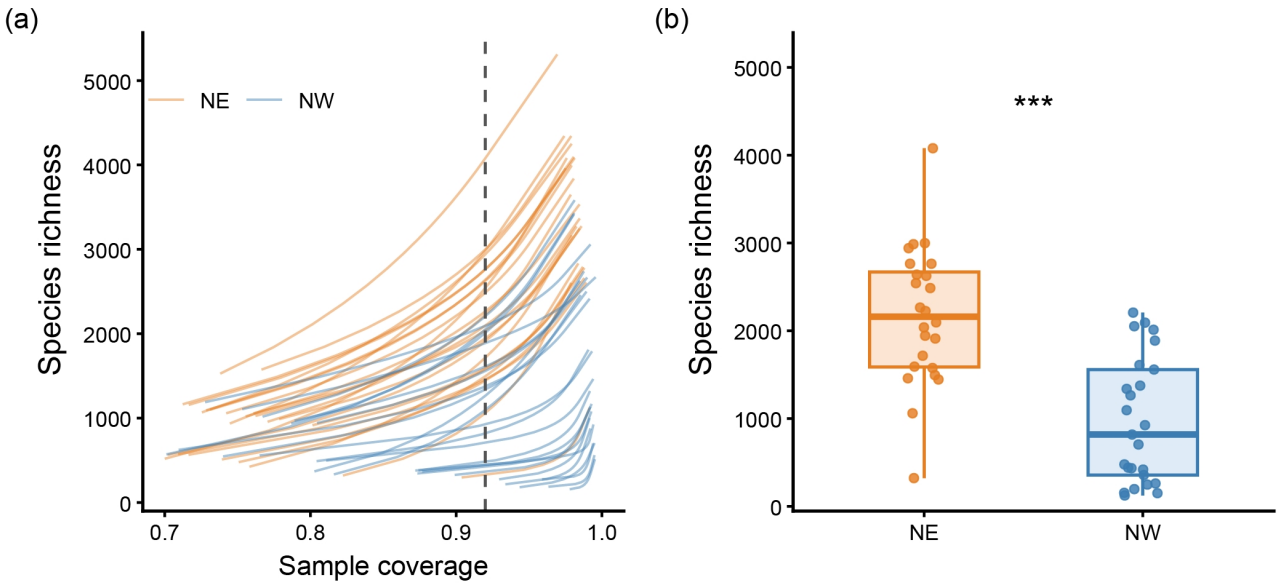


Fig. S2. Coverage-based bacterial species richness in NE and NW snow. (a) Sample coverage curves, with the dashed line marking 92% coverage. (b) Richness standardized to 92% coverage. *$p < 0.05$, **$p < 0.01$ and ***$p < 0.001$.

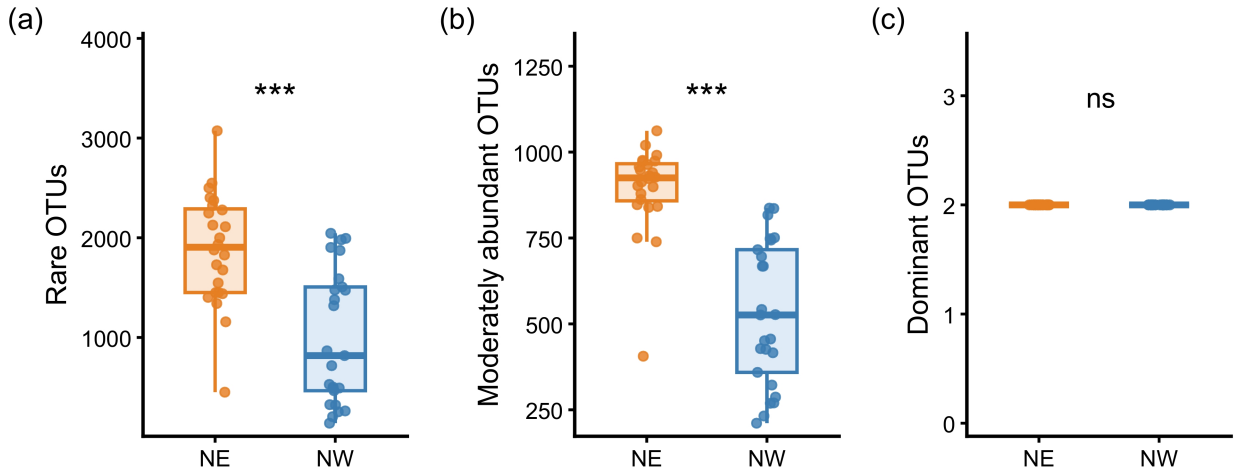


Fig. S3. Numbers of (a) rare, (b) moderately abundant, and (c) dominant bacterial OTUs in NE and NW. *$p < 0.05$, **$p < 0.01$ and ***$p < 0.001$.

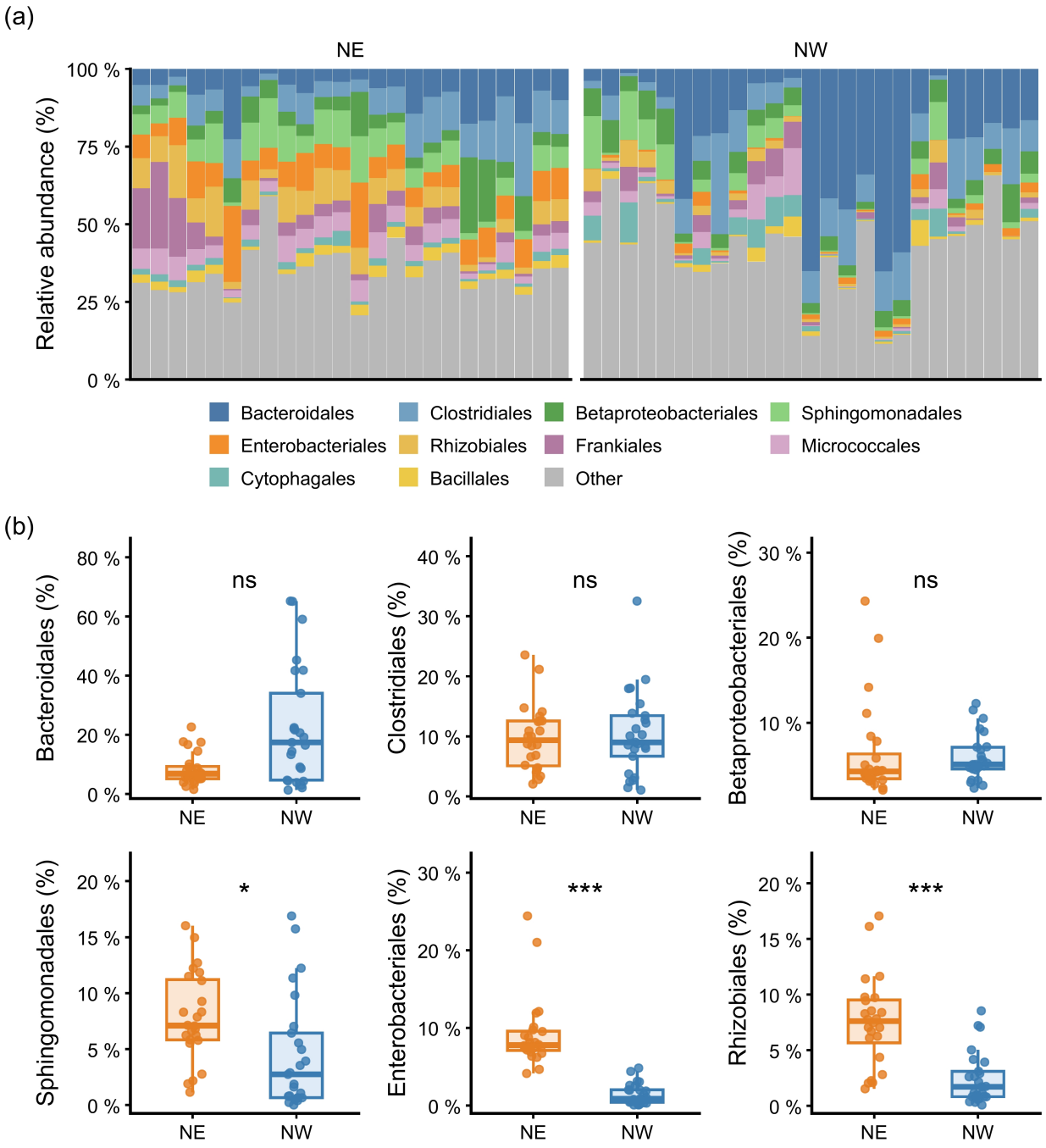


Fig. S4. Bacterial community composition at the order level in NE and NW snow. (a) Relative abundances by sample. (b) Mean relative abundances of the six dominant bacterial orders. Boxes show medians and interquartile ranges. *$p < 0.05$, **$p < 0.01$ and ***$p < 0.001$.

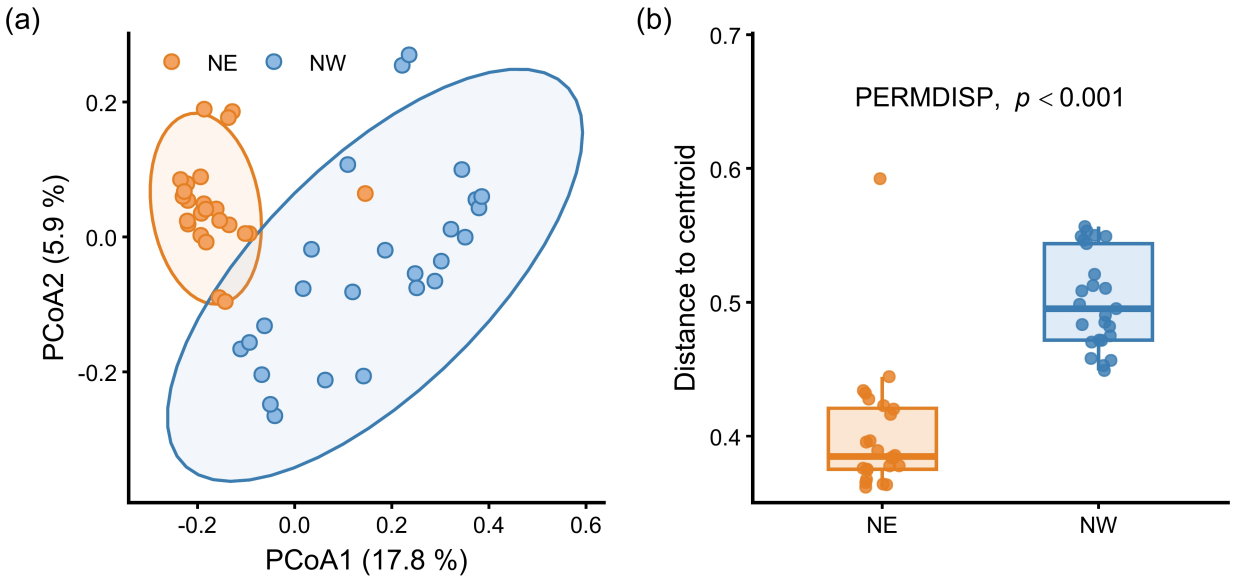


Fig. S5. Bacterial community composition and multivariate dispersion. (a) Principal coordinate analysis (PCoA) of unweighted UniFrac distances, with ellipses showing 95% confidence regions. (b) Distances to regional centroids from PERMDISP.

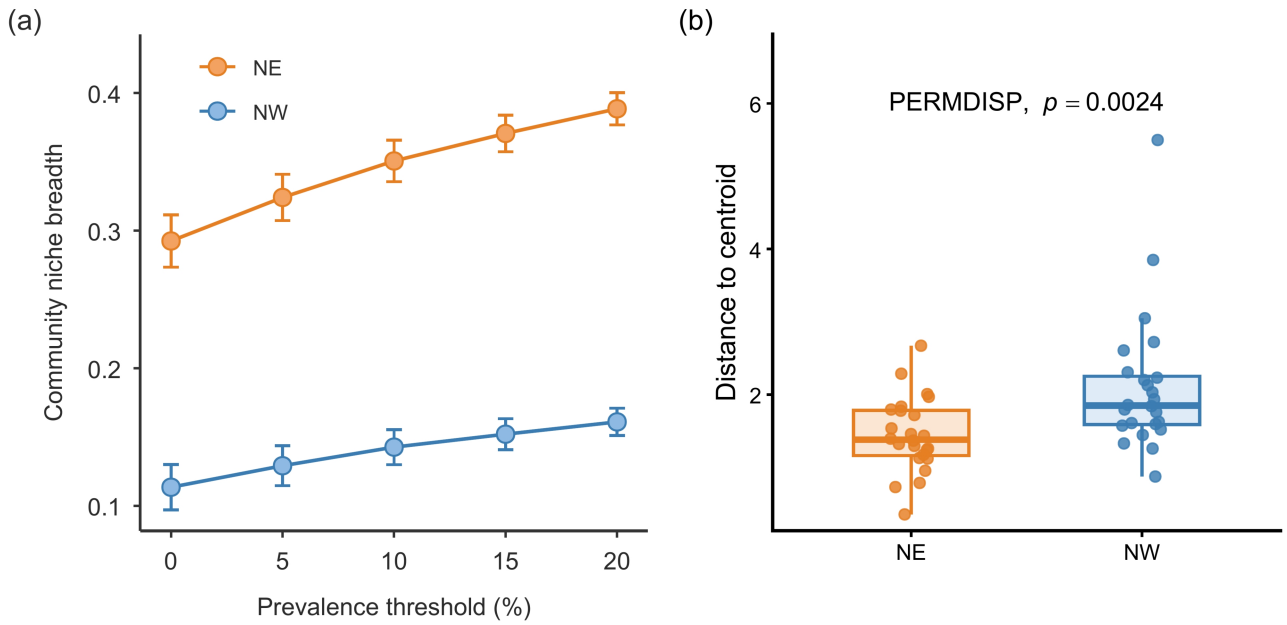


Fig. S6. (a) Community niche breadth across prevalence thresholds (mean ± SD). (b) Environmental distances to regional centroids from PERMDISP.

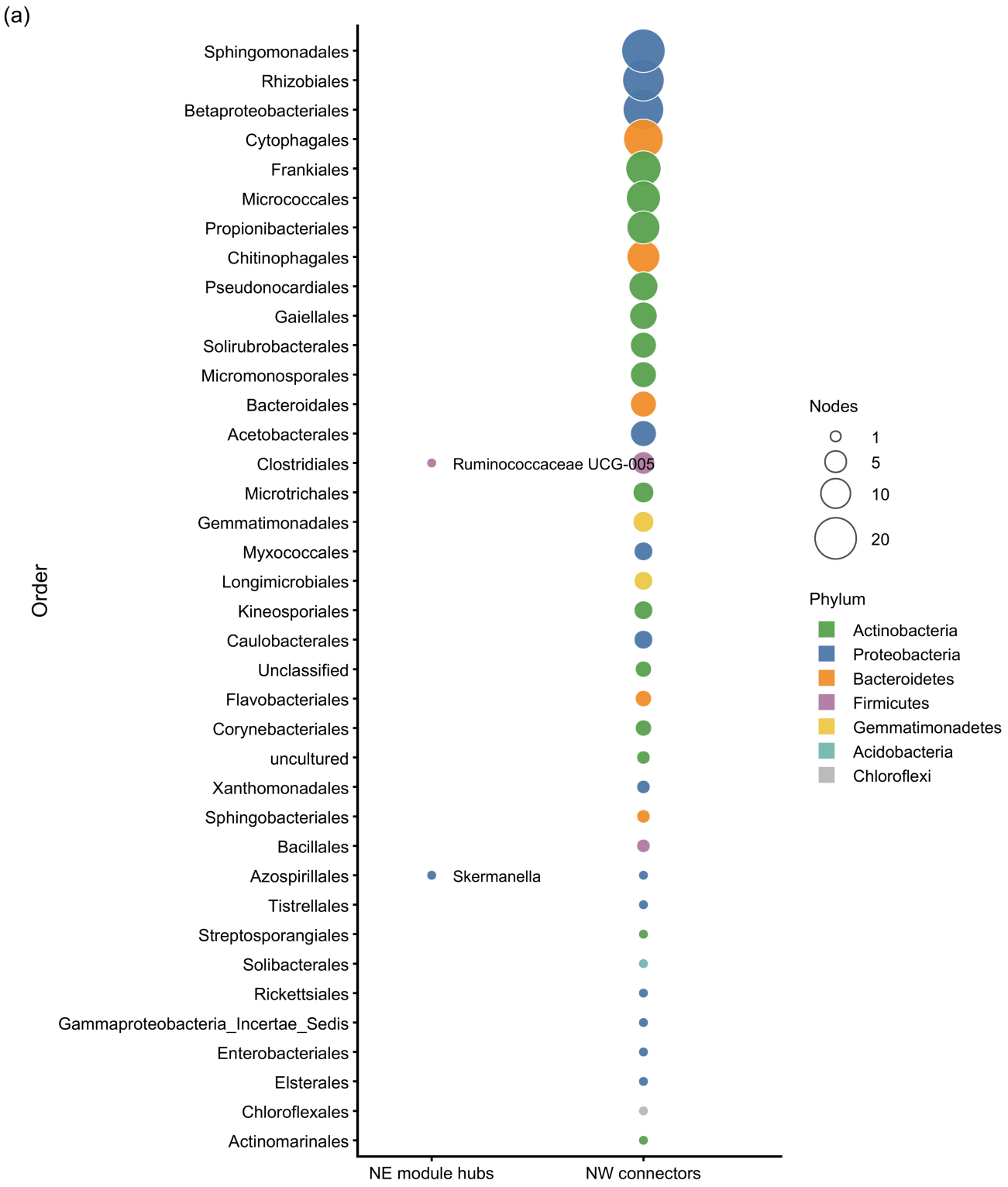


Fig. S7. Taxonomic composition of keystone nodes identified from Zi and Pi in the NE and NW networks. Bubble size denotes node count, and colour denotes phylum.

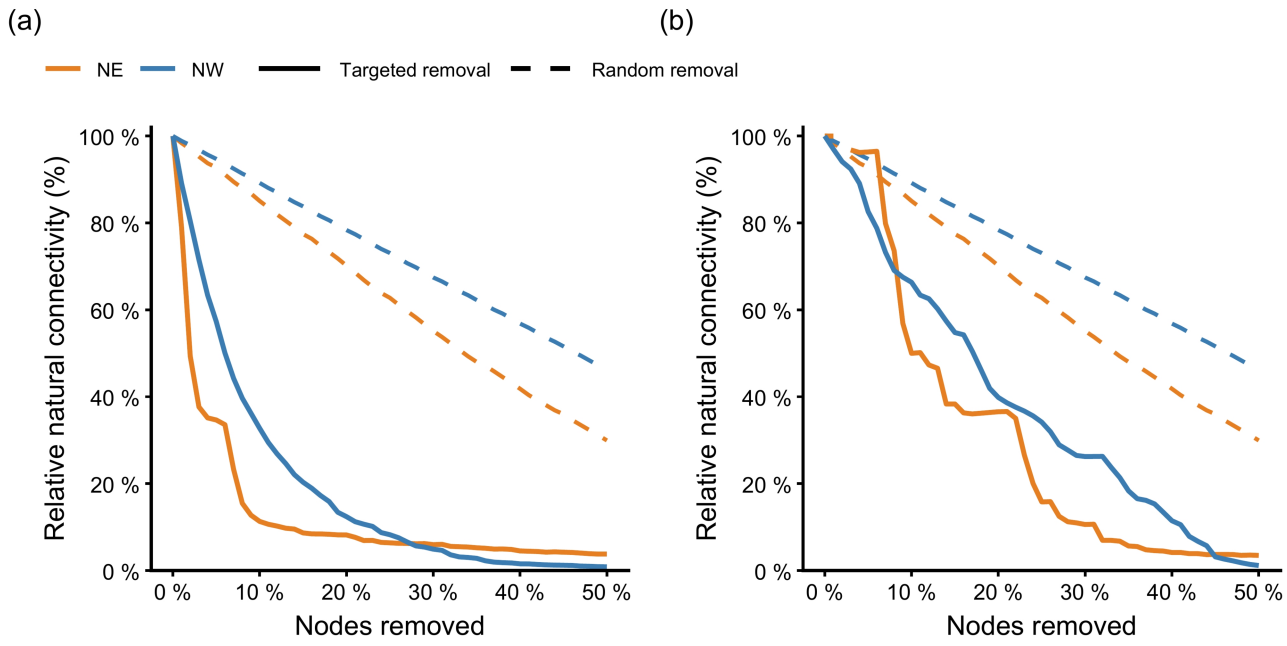


Fig. S8. Relative natural connectivity under (a) degree-targeted and (b) betweenness-targeted node removal. Dashed lines show random removal.

Table S1a. Sampling information and physical properties of surface snow samples from northeastern China (NE) and northwestern China (NW)

Sample ID	Site ID	Date	Latitude (° N)	Longitude (° E)	Elevation (m)	Air temperature (°C)	Wind speed ($m \cdot s^{-1}$)	Relative humidity (%)	Snow temperature (°C)	Snow density ($g \cdot mL^{-1}$)
NE.Q470	143	2020.12.27	44.389	125.961	205	-14.0	3.0	74.0	-9.0	0.180
NE.Q471	144	2020.12.27	44.530	126.395	157	-14.0	3.0	72.0	-12.0	0.133
NE.Q473	145	2020.12.28	44.943	127.507	196	-14.0	2.0	64.0	-15.0	0.150
NE.Q474	146	2020.12.28	45.308	126.760	177	-16.0	3.0	62.0	-14.0	0.260
NE.Q477	147	2020.12.29	46.351	126.792	142	-21.0	5.0	65.0	-21.0	0.150
NE.Q480	148	2020.12.30	47.356	127.309	229	-22.0	2.0	60.0	—	0.190
NE.Q481	149	2020.12.30	47.874	126.813	247	-18.0	4.0	52.0	—	0.230
NE.Q482	150	2020.12.31	48.052	125.071	240	-21.0	4.0	52.0	—	0.240
NE.Q483	151	2020.12.31	47.774	123.598	159	-17.0	1.0	35.0	—	0.180
NE.Q484	152	2021.1.1	46.671	124.476	132	-16.0	4.0	45.0	-13.0	0.330
NE.Q485	153	2021.1.2	45.914	125.997	122	-21.0	4.0	61.0	-21.0	0.210
NE.Q487	154	2021.1.3	45.664	124.862	147	-14.0	4.0	49.0	-5.0	0.280
NE.Q488	155	2021.1.3	45.282	125.139	134	-15.0	3.0	61.0	-12.0	0.200
NE.Q489	156	2021.1.4	44.692	124.977	255	-16.5	4.0	54.0	-17.0	0.270
NE.Q491	157	2021.1.4	44.314	125.025	168	-15.0	4.0	52.0	-12.0	0.200
NE.Q492	158	2021.1.4	44.083	125.025	182	-16.0	5.0	58.0	-18.0	0.200
NE.Q493	159	2021.1.5	43.905	124.316	160	-13.0	3.0	59.0	-12.0	0.230
NE.Q494	160	2021.1.5	44.005	123.134	154	-12.0	3.0	54.0	-12.0	0.290
NE.Q495	161	2021.1.6	43.219	121.827	227	-13.0	10.0	50.0	-14.0	0.270
NE.Q497	162	2021.1.6	43.187	120.600	342	-14.0	13.5	41.0	-10.0	0.200
NE.Q498	163	2021.1.7	42.963	121.363	306	-17.0	11.0	35.0	-14.0	0.210
NE.Q499	164	2021.1.7	43.500	121.589	208	-15.0	5.0	40.0	-11.0	0.220
NE.Q500	165	2021.1.8	43.511	122.819	176	-19.0	4.0	44.0	-15.0	0.220
NE.Q501	166	2021.1.8	43.774	124.980	237	-19.0	4.0	43.0	-11.0	0.190
NE mean ± SD	—	—	—	—	196 ± 56***	-16.4 ± 2.9*	4.5 ± 2.9***	53.4 ± 10.7	-13.4 ± 3.8	0.218 ± 0.048**
XJ.Q399	105	2018.01.09	45.695	83.055	1860	-3.0	2.0	53.0	-9.0	0.250
XJ.Q402	107	2018.01.10	45.016	82.599	190	-19.0	1.0	27.0	-8.0	0.120
XJ.Q403	108	2018.01.10	44.867	81.764	830	-13.0	1.0	53.0	-9.0	0.130
XJ.Q404	109	2018.01.11	44.563	82.526	330	-9.0	1.0	51.0	-9.0	0.120
XJ.Q405	110	2018.01.11	44.630	83.060	190	-18.0	2.0	64.0	-11.0	0.180
XJ.Q407	111	2018.01.12	44.584	83.616	340	-14.0	1.0	65.0	—	0.110
XJ.Q410	113	2018.01.13	44.278	85.395	640	-9.0	1.0	63.0	-6.0	0.220
XJ.Q412	114	2018.01.13	44.544	85.056	360	-14.0	1.0	72.0	-9.0	0.110
XJ.Q413	115	2018.01.14	44.040	86.758	820	-8.0	2.0	63.0	-6.0	0.180
XJ.Q414	116	2018.01.14	43.776	87.254	940	-14.0	0.0	72.0	—	0.120
XJ.Q416	117	2018.01.15	43.522	87.314	1570	-4.0	3.0	40.0	-7.0	0.120
XJ.Q418	118	2018.01.15	43.629	87.527	1192	-13.0	8.0	76.0	-9.0	0.250
XJ.Q420	119	2018.01.16	44.221	88.706	560	-11.0	2.0	54.0	-12.0	0.100
XJ.Q421	120	2018.01.17	46.508	89.568	910	-27.0	1.0	58.0	-29.0	0.120
XJ.Q423	121	2018.01.17	47.204	88.564	945	-13.0	3.0	50.0	-12.0	0.160
XJ.Q424	122	2018.01.18	47.456	87.381	500	-19.0	2.0	55.0	-14.0	0.180
XJ.Q425	123	2018.01.18	47.889	86.284	450	-13.0	4.0	63.0	-11.0	0.210
XJ.Q426	124	2018.01.19	47.286	86.271	1120	-14.0	1.0	57.0	-12.0	0.210
XJ.Q427	125	2018.01.19	46.855	86.309	1200	-8.0	1.0	—	-11.0	0.200
XJ.Q428	126	2018.01.19	46.868	85.686	1550	-8.0	2.0	52.0	-13.0	0.210
XJ.Q429	127	2018.01.20	46.383	85.935	690	-13.0	1.0	33.0	-13.0	0.190
XJ.Q430	128	2018.01.20	45.951	85.498	330	-14.0	1.0	64.0	-13.0	0.160
XJ.Q431	129	2018.01.21	45.472	85.457	290	-16.0	2.0	38.0	-11.0	0.130
XJ.Q432	130	2018.01.21	45.226	87.755	550	-14.0	1.0	40.0	-28.0	0.220
XJ.Q433	131	2018.01.22	44.037	89.625	750	-15.0	1.0	45.0	-13.0	0.190
NW mean ± SD	—	—	—	—	764 ± 454	-13.0 ± 5.1	1.7 ± 1.5	54.5 ± 12.5	-11.9 ± 5.7	0.168 ± 0.047

Table S1b. Chemical properties of surface snow samples from northeastern China (NE) and northwestern China (NW)

Sample ID	TOC ($mg \cdot L^{-1}$)	Na^+ ($mg \cdot L^{-1}$)	NH_4^+ ($mg \cdot L^{-1}$)	K^+ ($mg \cdot L^{-1}$)	Mg^{2+} ($mg \cdot L^{-1}$)	Ca^{2+}($mg \cdot L^{-1}$)	Cl^- ($mg \cdot L^{-1}$)	SO_4^{2-} ($mg \cdot L^{-1}$)	NO_3^- ($mg \cdot L^{-1}$)
NE.Q470	30.672	2.202	5.148	1.196	0.636	7.103	4.374	20.131	6.352
NE.Q471	14.027	0.994	2.311	0.792	0.359	4.158	1.894	9.580	3.020
NE.Q473	15.403	1.034	2.667	1.780	0.571	6.337	2.426	12.802	5.132
NE.Q474	23.123	0.700	3.732	0.806	0.342	3.893	1.864	10.513	4.459
NE.Q477	12.370	0.446	4.221	0.813	0.311	3.435	1.390	10.407	3.563
NE.Q480	10.252	0.083	0.450	0.235	0.089	0.957	0.461	1.659	2.292
NE.Q481	12.693	0.085	0.519	0.276	0.159	1.055	0.437	1.911	2.558
NE.Q482	17.824	0.134	0.907	0.423	0.245	1.245	0.491	2.952	2.034
NE.Q483	17.205	0.092	1.362	0.489	0.195	1.144	0.596	2.133	2.992
NE.Q484	24.341	32.638	0.719	1.331	2.785	3.474	15.695	23.899	3.640
NE.Q485	17.716	0.386	2.171	0.634	0.645	3.706	0.750	6.461	1.444
NE.Q487	19.900	0.804	1.294	0.596	0.634	6.596	0.632	4.349	1.192
NE.Q488	39.793	1.144	2.304	0.799	0.447	5.800	1.980	10.478	2.095
NE.Q489	14.088	0.404	1.162	0.406	0.207	2.782	0.614	3.457	1.176
NE.Q491	13.351	0.711	2.942	0.711	0.362	4.073	1.391	8.796	2.168
NE.Q492	17.030	1.024	3.587	0.864	0.457	5.247	1.967	12.523	2.945
NE.Q493	23.973	0.745	2.821	0.619	0.385	4.368	1.245	9.873	2.435
NE.Q494	13.629	0.560	1.861	0.616	0.399	4.922	0.856	5.967	1.099
NE.Q495	14.730	0.315	0.999	0.565	0.347	6.492	0.417	7.318	1.124
NE.Q497	24.183	0.292	0.569	0.235	0.145	1.981	0.432	3.504	0.667
NE.Q498	8.669	0.146	0.475	0.183	0.121	1.734	0.217	2.623	0.581
NE.Q499	18.708	0.342	1.255	0.734	0.357	5.323	0.506	6.940	1.119
NE.Q500	9.600	0.378	1.959	0.614	0.232	2.960	0.537	5.465	1.056
NE.Q501	20.042	1.127	3.342	0.941	0.502	6.019	2.239	12.578	2.840
NE mean ± SD	18.055 ± 7.079***	1.949 ± 6.554	2.032 ± 1.308*	0.694 ± 0.366***	0.456 ± 0.522**	3.950 ± 1.931	1.809 ± 3.108	8.180 ± 5.608*	2.416 ± 1.455
XJ.Q399	0.899	0.152	0.087	0.132	0.070	1.351	0.137	0.455	0.532
XJ.Q402	4.429	1187.686	3.898	25.605	185.848	57.302	448.935	995.548	12.784
XJ.Q403	1.346	0.387	0.992	0.248	0.207	4.838	1.384	4.732	3.574
XJ.Q404	1.958	0.746	1.280	0.349	0.409	8.850	1.034	15.098	6.196
XJ.Q405	1.451	2.975	0.884	0.236	0.189	2.740	2.331	8.151	5.719
XJ.Q407	1.561	0.427	0.910	0.207	0.185	2.640	0.706	3.685	6.967
XJ.Q410	2.558	0.605	3.455	0.344	0.169	3.946	1.093	8.818	5.313
XJ.Q412	2.228	1.194	3.627	0.445	0.323	4.563	2.144	11.671	7.948
XJ.Q413	0.776	0.189	2.690	0.261	0.082	1.908	0.578	4.982	3.229
XJ.Q414	2.290	1.604	2.524	0.428	0.469	10.479	2.256	8.867	2.868
XJ.Q416	1.384	0.243	0.715	0.173	0.180	2.993	0.307	1.935	1.351
XJ.Q418	2.461	3.753	1.759	0.549	1.546	11.044	6.738	15.471	3.735
XJ.Q420	0.878	0.164	0.928	0.183	0.038	0.447	0.377	0.040	2.562
XJ.Q421	7.069	0.082	0.065	0.082	0.020	0.408	0.101	0.409	0.889
XJ.Q423	0.616	0.237	0.144	0.118	0.045	0.349	0.353	0.797	1.163
XJ.Q424	0.980	0.160	0.374	0.185	0.088	1.041	0.247	1.701	2.495
XJ.Q425	0.671	0.042	0.080	0.098	0.028	0.326	0.105	0.494	1.296
XJ.Q426	0.478	0.053	0.101	0.096	0.015	0.330	0.101	0.462	1.045
XJ.Q427	0.566	0.094	0.161	0.123	0.040	1.160	0.115	0.496	0.829
XJ.Q428	1.241	0.096	0.044	0.177	0.078	1.995	0.075	0.547	0.619
XJ.Q429	1.099	0.720	0.237	0.207	0.065	1.083	1.046	1.086	2.655
XJ.Q430	1.637	0.312	0.287	0.160	0.046	0.544	0.497	1.167	3.406
XJ.Q431	1.135	0.164	0.519	0.214	0.107	1.189	0.331	1.552	3.979
XJ.Q432	0.791	0.149	0.305	0.182	0.092	1.175	0.450	1.352	4.376
XJ.Q433	3.085	2.039	4.322	0.608	0.500	5.467	3.310	16.116	5.918
NW mean ± SD	1.744 ± 1.442	48.171 ± 237.401	1.216 ± 1.370	1.256 ± 5.075	7.634 ± 37.129	5.127 ± 11.304	18.990 ± 89.584	44.225 ± 198.261	3.658 ± 2.849

Table S2. Bacterial OTU richness by abundance class

Abundance class	NE mean	NW mean	Difference NE − NW	95% CI	Adjusted *p*	Rank biserial *r*
Dominant (≥ 1%)	2.00	2.00	0.00	—	—	—
Moderately abundant (0.01% ≤ abundance < 1%)	894.33	528.12	366.21	274.17 to 457.80	<0.001	0.907
Rare (< 0.01%)	1886.04	997.16	888.88	571.85 to 1199.16	<0.001	0.650

Table S3. Differential abundance of selected bacterial taxa between northeastern China (NE) and northwestern China (NW)

Taxonomic rank	Taxon	NE relative abundance (%)	NW relative abundance (%)	Log_2 fold change	Wilcoxon adjusted *p*	ALDEx2 effect	ALDEx2 adjusted *p*
Class	Bacteroidia	13.54	30.94	-1.192	<0.001	0.880	<0.001
Family	Muribaculaceae	1.98	10.18	-2.361	0.004	0.919	0.002
Family	Rikenellaceae	0.70	2.66	-1.922	0.009	0.951	0.002
Genus	*Alistipes*	0.25	1.75	-2.794	<0.001	1.410	<0.001
Genus	*Alloprevotella*	0.21	1.51	-2.840	0.005	1.107	<0.001
Order	Enterobacteriales	9.19	1.44	2.670	<0.001	-0.962	<0.001
Family	Enterobacteriaceae	9.19	1.44	2.670	<0.001	-0.743	0.011
Order	Rhizobiales	7.57	2.46	1.622	<0.001	-0.848	0.001

Note. Positive log_2 fold-change values indicate higher abundance in NE. Positive ALDEx2 effects indicate higher abundance in NW.

Table S4. Full, selected, and partial RDA results

Model	Term	n	R^2	Adjusted R^2	Pseudo F	p	Contribution (%)
Full model	Overall	42	0.356	0.200	2.284	0.0001	
Selected model	Overall	42	0.293	0.194	2.977	0.0001	
	TOC				3.663	0.0001	50.5
	Air temperature				1.937	0.012	13.6
	Ca^{2+}				1.868	0.016	19.0
	NO_3^-				1.727	0.025	11.7
	Relative humidity				1.522	0.054	5.3
Partial model	Overall	42	0.169	0.075	1.758	0.0001	
	TOC				0.869	0.724	
	Air temperature				1.765	0.006	
	Ca^{2+}				1.922	0.003	
	NO_3^-				1.675	0.010	
	Relative humidity				1.575	0.017	

Note. All analyses used 42 complete samples. The full model included air temperature, wind speed, relative humidity, snow temperature, snow density, TOC, Ca^{2+}, and NO_3^-. The partial model was conditioned on region.

Table S5. Sensitivity analyses of the RDA model

Model	n	Predictors	Adjusted R^2	Pseudo F	p
Model 1	49	TOC, Air temperature, Ca^{2+}, NO_3^-	0.171	3.481	<0.001
Model 2	48	TOC, Air temperature, Ca^{2+}, NO_3^-, Relative humidity	0.182	3.086	<0.001
Model 3	41	TOC, Air temperature, Ca^{2+}, NO_3^-, Relative humidity	0.197	2.962	<0.001
Model 4	41	TOC, Air temperature, Wind speed	0.171	3.744	<0.001

Note. Model 1 used all 49 samples without relative humidity; Model 2 used 48 complete samples; Models 3–4 excluded XJ.Q402 from the 42 sample data set in Table S4. Model 4 repeated collinearity screening and forward selection.

Table S6. Properties of the NE and NW bacterial networks

Network property	NE	NW
Nodes	290	669
Edges	533	11616
Mean degree	3.676	34.726
Density	0.0127	0.0520
Diameter	14	11
Mean path length	6.376	2.910
Mean clustering coefficient	0.232	0.385
Modularity	0.776	0.142

References

Amoroso, A., Domine, F., Esposito, G., Morin, S., Savarino, J., Nardino, M., Montagnoli, M., Bonneville, J.-M., Clement, J.-C., and Ianniello, A.: Microorganisms in dry polar snow are involved in the exchanges of reactive nitrogen species with the atmosphere, Environ. Sci. Technol., 44, 714–719, https://doi.org/10.1021/es9027309, 2010.

Fourtziou, L., Liakakou, E., Stavroulas, I., Theodosi, C., Zarmpas, P., Psiloglou, B., Sciare, J., Maggos, T., Bairachtari, K., Bougiatioti, A., Gerasopoulos, E., Sarda-Estève, R., Bonnaire, N., and Mihalopoulos, N.: Multi-tracer approach to characterize domestic wood burning in Athens (Greece) during wintertime, Atmos. Environ., 148, 89–101, https://doi.org/10.1016/j.atmosenv.2016.10.011, 2017.

Grannas, A. M., Shepson, P. B., and Filley, T. R.: Photochemistry and nature of organic matter in Arctic and Antarctic snow, Global Biogeochem. Cycles, 18, GB1006, https://doi.org/10.1029/2003GB002133, 2004.

Liu, Y., Fang, P., Guo, B., Ji, M., Liu, P., Mao, G., Xu, B., Kang, S., and Liu, J.: A comprehensive dataset of microbial abundance, dissolved organic carbon, and nitrogen in Tibetan Plateau glaciers, Earth Syst. Sci. Data, 14, 2303–2314, https://doi.org/10.5194/essd-14-2303-2022, 2022.

Luo, L., Wu, Y., Xiao, H., Zhang, R., Lin, H., Zhang, X., and Kao, S.-j.: Origins of aerosol nitrate in Beijing during late winter through spring, Sci. Total Environ., 653, 776–782, https://doi.org/10.1016/j.scitotenv.2018.10.306, 2019.

Mu, Z., Ma, Y., Wen, H., Zhang, C., Qi, Y., Zhang, D., Zhou, Y., Pu, W., and Wang, X.: The Spatial Distribution of Dissolved Organic Matter and Its Molecular Fingerprints in Seasonal Snow Over Northeastern China, J. Geophys. Res. Atmos., 128, e2023JD039117, https://doi.org/10.1029/2023JD039117, 2023.

Murphy, K. R., Stedmon, C. A., Waite, T. D., and Ruiz, G. M.: Distinguishing between terrestrial and autochthonous organic matter sources in marine environments using fluorescence spectroscopy, Mar. Chem., 108, 40–58, https://doi.org/10.1016/j.marchem.2007.10.003, 2008.

Zatko, M., Geng, L., Alexander, B., Sofen, E., and Klein, K.: The impact of snow nitrate photolysis on boundary layer chemistry and the recycling and redistribution of reactive nitrogen across Antarctica and Greenland in a global chemical transport model, Atmos. Chem. Phys., 16, 2819–2842, https://doi.org/10.5194/acp-16-2819-2016, 2016.